Modeling of tunnel diode oscillators

Craig T. Van Degrift

Temperature and Pressure Measurements and Standards Division, Center for Absolute Physical Quantities, National Bureau of Standards, Washington, D.C. 20234

David P. Love

Department of Physics, Texas A & M University, College Station, Texas 77843

The detailed behavior of tunnel diode LC oscillators is calculated by three different methods and compared with experiment. We present both analytic formulas and numerical methods which give corrections to the oscillator frequency calculated using the expression $1/(LC)^{1/2}$ and show that these corrections are often not negligible. The calculations also yield rf amplitude, bias current dependence, and other details necessary for the full realization of the performance of LC oscillators as transducers of pressure, temperature, and other physical quantities.

PACS numbers: 84.30.Ft, 85.30.Mn

INTRODUCTION

There have been many experiments, primarily at low temperatures, in which tunnel diode oscillators have been used to measure a primary experimental quantity. For example, they have been used to measure pressure,[1–6] dielectric constant,[7–10] He-3 concentration,[11,12] liquid level,[13,14] plasma sheath capacitance,[15] ordinary rf susceptibility,[16–22] NMR susceptibility,[23–25] magnetic specific heat,[26] kinetic inductance,[27,28] penetration depth,[29,30] skin depth,[30] transition radiation,[31] and neutron flux.[32] Sometimes they are used as thermometers.[4,16,18,19,22] Invariably, the experimenter will assume that the oscillator frequency varies as $1/(LC)^{1/2}$ and make rough arguments to justify the ignorance of corrections to this formula. Although, as we show later, this is often correct, we feel that it is important to examine these corrections with greater care than has been done previously by experimentalists[7,9,17,29] and presented in engineering texts[33–38] and with greater emphasis on transducer applications than has been done in existing theoretical treatments.[39–43] The work reported in this paper was inspired by an experiment[30] to measure the surface impedance of high purity metallic rods suspended within the inductor of a tunnel diode oscillator. In that experiment the Q-dependent corrections have turned out to be about 5%—small but still significant.

The proper design of high performance tunnel diode oscillators also requires a better understanding of the nonlinear effects discussed in this paper. An earlier paper[44] gave rules adequate for low-frequency ($f < 20$ MHz) oscillators with 0.001 ppm frequency stability, but restricted its mathematical discussion to the behavior very close to the threshold of oscillation. The extent to which those rules applied for stronger oscillations was not indicated. That weakness is remedied in this paper. The tools which we present here can also be used in the analysis of high-frequency circuits (20 MHz $< f < 2$ GHz) utilizing reentrant LC resonators,[45] and can form the basis for a detailed analysis of noise effects.

Whereas our discussion is given in terms of LC oscillators which use tunnel diodes as the gain element, it is actually more broadly applicable since all oscillators possess similar properties.

In the next section, we describe a general tunnel diode oscillator circuit which can be used to represent low-frequency oscillators with tapped or untapped multiturn inductors or high-frequency oscillators coupled to reentrant LC resonators. The following sections describe three methods for modeling the circuit. The first method is a full numerical simulation using a large digital computer. Since this method is very time consuming and expensive, we then present an approximate numerical analysis method which is appropriate for use with a microcomputer.[46] Finally, we describe an analytical approximation which produces formulas suitable for computation on a pocket calculator. The results of all methods are compared with each other and with measurements on an actual oscillator.[30] While the specific calculations are carried out for a low-frequency multiturn inductor oscillator, they apply quite well to high-frequency reentrant resonator oscillators when an equivalent to the tapping fraction is used to represent the coupling coefficient between the resonator and the diode. We will, however, defer to a future paper the specific subject of reentrant resonator tunnel diode oscillators.

I. GENERAL EQUIVALENT CIRCUIT

A general equivalent circuit which applies to a wide variety of tunnel diode oscillators is shown in Fig. 1. The dc bias current, I_{bias}, divides between the dc load resistor, R_B, and the series circuit consisting of the tunnel diode, parasitic suppression resistor, R_p, and the lower half of the inductor. A voltage, V_{bias}, appears across the circuit while, in the absence of rf oscillation, a smaller voltage, V_{do}, appears across the tunnel diode and a current, I_{do}, passes through it. When there is rf oscillation the dc bias conditions are slightly altered due to a self-rectification of the rf currents by the diode.

Downloaded 25 May 2011 to 128.227.27.199. Redistribution subject to AIP license or copyright; see http://rsi.aip.org/about/rights_and_permissions

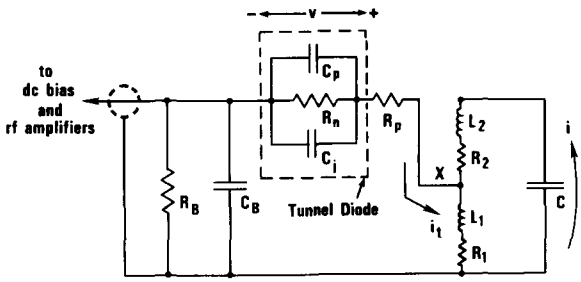

FIG. 1. The general circuit of a tunnel diode oscillator with a tapped LC resonator. The components R_n, C_j, and part of C_p represent the tunnel diode.

This causes a hysteresis in the behavior of the circuit as the dc bias is changed.

The main LC circuit is represented by a tapped inductance, $L = L_1 + L_2 + 2M_L$, and a capacitance, C. The quality factor, Q, of the resonator is given by $Q = \omega_0 L/R$, where $\omega_0 = 2\pi f_0 = 1/(LC)^{1/2}$, and $R = R_1 + R_2 + 2M_R$ is the sum of the resistances, R_1 and R_2, representing losses associated with the inductor. M_L and M_R represent the mutual inductance and resistance between the parts of the inductor. The precise definition of the tapping fraction, x, depends upon the type of analysis being performed and will be covered later.

The dc $I-V$ curve of the tunnel diode defines V_{do} and a differential resistance, R_{no}, as functions of I_{do}. The instantaneous differential resistance, R_n, and junction capacitance, C_j, are determined from the instantaneous voltage across the tunnel diode.

The usual microwave equivalent circuit for the tunnel diode also has a series resistance and a series inductance. We have lumped the series resistance together with the negative resistance, and consider the series inductance negligible for the low-power (<100 μW) tunnel diodes we are using. It will not be difficult to include these additional components into the numerical simulation or numerical approximation analyses when high-frequency oscillators are considered and good measurements of their values are available. For this paper, however, we will not consider these components. Similarly, we will neglect an inductance in series with R_p which is likely to be important only at higher frequencies. The capacitance, C_p, shunting the tunnel diode represents the parallel combination of the case capacitance of the tunnel diode and any intentional shunt capacitance added to help R_p reduce the high-frequency gain of the circuit and thereby suppress certain parasitic oscillations.[47]

Finally, to achieve good isolation from external noise and impedance changes, the bypass capacitor, C_B, is chosen to have an impedance several orders of magnitude lower than R_n. For very low-frequency (<2 MHz) oscillators, C_B is actually replaced by a network to avoid the need for unreasonable values of capacitance.[30] In this paper we can neglect it in our calculations. It need only be considered when calculating the rf output signal voltage from the rf diode current.

II. NUMERICAL SIMULATION

The numerical simulation is a straightforward, brute-force integration of the simultaneous nonlinear differential equations describing the circuit. It is accurate and makes few assumptions but is quite time consuming, expensive, and requires a large digital computer. A well-developed FORTRAN subroutine named DVDQ[48] performs the integration. DVDQ is called by our smaller main program TDO, which has small subroutines for inductance calculations, interpolation, and Fourier analysis.

TDO first reads the circuit parameters including the measured $I-V$ curve data for the specific tunnel diode being considered. From the precise geometry of the inductor it then calculates[49] the total inductance, L, and the separate inductances L_1 and L_2 shown in Fig. 1. The mutual inductance between L_1 and L_2 is given by $M_L = (L - L_1 - L_2)/2$ and the tapping fraction by $x = (L_1 + M_L)/L$. Using a specified quality factor, Q, TDO then calculates the total rf resistance, R. The separate resistances, R_1 and R_2, and mutual resistance M_R are assumed to be the same fraction of R as L_1, L_2, and M_L are of L.

There are three coupled differential equations which govern the behavior of the circuit when C_B is considered an rf short circuit. These equations may be written using three variables v, i_t, and i: v is the voltage across the diode in excess of the applied dc bias voltage; i_t is the current through resistor R_p into the tap of the inductor in excess of the applied dc bias; and i is the current through the main capacitance, C. These currents are shown in Fig. 1. By inspection one may write the loop equations as

$$(L_1 + M_L)\frac{d(i + i_t)}{dt} + (R_1 + M_R)(i + i_t) + (L_2 + M_L)\frac{di}{dt} + (R_2 + M_R)i + \frac{1}{C}\int i\,dt = 0, \quad (1)$$

$$L_1\frac{d(i + i_t)}{dt} + R_1(i + i_t) + M_L\frac{di}{dt} + M_R i + R_p i_t = v, \quad (2)$$

and

$$-\frac{d}{dt}\{[C_p + C_j(v + V_{do})](v + V_{do})\} - I_d(v + V_{do}) + I_{do} = i_t, \quad (3)$$

where

$$C_j(v + V_{do}) = C_{jo}/[1 - (v + V_{do})/V_{jo}]^{1/2}. \quad (4)$$

In Eq. (4), the depletion capacitance relation for the tunnel diode, C_{jo} is the zero voltage junction capacitance, and V_{jo} is the band gap voltage. The value of C_{jo} is usually between 0.1 and 3 pF, but can be very different for diodes which are otherwise similar. The value for V_{jo}, on the other hand, is a property of the semiconductor material and for germanium can be considered to be 600 mV, roughly independent of temperature.

Downloaded 25 May 2011 to 128.227.27.199. Redistribution subject to AIP license or copyright; see http://rsi.aip.org/about/rights_and_permissions

Equations (1)–(3) must be rearranged and the variables changed slightly to make them more suitable for the numerical analysis. It is more convenient to calculate the corresponding charges and their derivatives than to use currents. We therefore introduce the variables q and q_t which are related to i and i_t by simple differentiation with respect to time. It is also convenient to introduce functions $F(v)$ and $G(v)$ defined by

$$F(v) = I_d(v + V_{do}) - I_d(V_{do}) = I_d(v + V_{do}) - I_{do}, \quad (5)$$

and

$$G(v) = \frac{d}{dv}\{[C_p + C_j(v + V_{do})](v + V_{do})\}. \quad (6)$$

The basic differential equations may now be rewritten in the form

$$q'' = -\frac{x}{L^*}v + \frac{xR_p}{L^*}q_t' - \frac{x^2}{L^*C}q - \frac{R}{L}q' - \frac{q}{LC}, \quad (7)$$

$$q_t'' = \frac{1}{L^*}v - \left(\frac{R_p}{L^*} + \frac{R}{L}\right)q_t' + \frac{x}{L^*C}q, \quad (8)$$

and

$$v' = -[F(v) + q_t']/G(v), \quad (9)$$

where the notation L^* is used to represent L_1-x^2L, a frequent denominator. The highest order derivatives of each variable have been written on the left-hand side of these equations as required by DVDQ. Values for variables on the left-hand side at time $t + dt$ are calculated from values for the variables on the right-hand side at time t. In deriving Eqs. (7) and (8), we have made use of the assumption that $R_1/L_1 = R_2/L_2 = M_R/M_L = R/L$.

For the case when the diode is directly coupled to the top of the LC resonator, $x = 1$ and L^* diverges. If R_p is still nonzero,[50] we have three new equations. Starting with Eqs. (1)–(3) and using a variable $q_1 = q + q_t$ in place of q_t, but otherwise following similar steps as before, we obtain:

$$q_1'' = -\frac{R}{L}q_1' - \frac{1}{LC}q, \quad (10)$$

$$q' = q_1' - \frac{1}{R_p}v - \frac{1}{R_pC}q, \quad (11)$$

and

$$v' = -[F(v) - q' + q_1']/G(v). \quad (12)$$

If there is no parasitic suppression resistor, $R_p = 0$, and the variables v and q are redundant since $v = -q/C$. We are left with only two equations:

$$q_1'' = -\frac{R}{L}q_1' + \frac{1}{L}v, \quad (13)$$

and

$$v' = -[F(v) + q_1']/[G(v) + C]. \quad (14)$$

The integration is started by first setting the dc bias to the point of minimum magnitude of negative resistance, initializing the current through the capacitor to a plausible value, setting all other variables and derivatives to zero, and guessing Q to be $R_{no}/x^2\omega_0L$, where R_{no} is the minimum magnitude of the negative resistance of the tunnel diode. After integrating for four cycles, the growth or decline of the amplitude is used to provide a better guess of the Q according to the following relation:

$$\frac{1}{Q_{\text{new}}} = \frac{1}{Q_{\text{old}}} + \frac{q_{\text{new}}' - q_{\text{old}}'}{\pi q_{\text{old}}'}, \quad (15)$$

where q'_{new} and q'_{old} represent the peak positive excursions of q' during the present and previous cycles, respectively. All amplitudes of variables and derivatives are then scaled by a factor which leaves the maximum excursion of the rf voltage across the diode, $v_{\max}$, at 1.00 mV. Two more complete cycles of oscillation are integrated followed by a further scaling of the amplitudes. This two cycle integration and scaling process is repeatedly performed until the Q values change by less than 0.01%. The Q and frequency shift from f_0 are then considered to correspond to the true values at the threshold of oscillation (limit as $v_{\max} \to 0$).

A full simulation of a circuit consists of calculation of the Q's and frequency shifts for a mesh of values of V_{do} and $v_{\max}$ which spans the region of interest. For each point in the mesh, Fourier analyses[51] of the currents i_t and i and voltage v are made using 100 sample points of a cycle of the steady-state solution. The dc components of i_t and v, i_{to} and v_0, are used to calculate the true circuit dc bias parameters, I_{bias} and V_{bias}, using the following equations:

$$V_{\text{bias}} = V_{do} + v_o + (I_{do} + i_{to})R_p, \quad (16)$$

$$I_{\text{bias}} = I_{do} + i_{to} + V_{\text{bias}}/R_B. \quad (17)$$

The amplitude of the fundamental component of i_t allows calculation of the rf output voltage using C_B and R_B, while the amplitude of the fundamental component of i allows calculation of the rf magnetic field applied to a sample which might be placed within the inductor. A two-dimensional interpolation over the calculated points on the mesh finally allows these rf amplitudes, the Q, and the fractional frequency shift from f_0 to be calculated as a functions of I_{bias} and of each other.

III. ASSUMPTIONS USED IN THE NUMERICAL SIMULATION

It is useful to declare explicitly the assumptions used during the numerical simulation at this time: (1) The impedance of C_B is small enough that i_t can be calculated adequately by neglecting R_B, C_B, and any reactances external to the circuit. (2) The series resistance and series inductance within the tunnel diode package can be neglected. (3) All losses in the LC resonator occur in the inductor and are distributed in the same ratio as L_1, L_2, and M_L. (4) The dc resistance of the inductor is negligible. (5) There is no parasitic oscillation.

Downloaded 25 May 2011 to 128.227.27.199. Redistribution subject to AIP license or copyright; see http://rsi.aip.org/about/rights_and_permissions

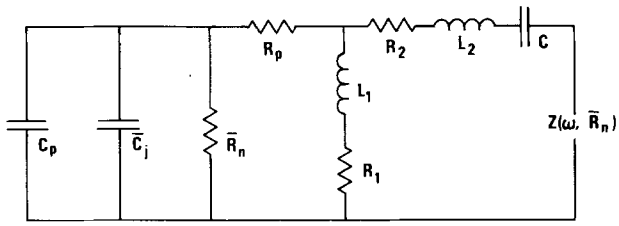

FIG. 2. The ac equivalent circuit used for the numerical and analytical approximation calculations. Zeros of the impedance $Z(\omega, \overline{R_n})$ determine the frequency and amplitude of oscillation.

IV. NUMERICAL APPROXIMATION

The methods we shall call numerical approximation and analytical approximation are based on the commonly used engineering approach of looking for a zero in the open-circuit impedance of the resonator.[52] Figure 2 shows the equivalent circuit for the impedance to be calculated. The notations $\overline{C_j}$ and $\overline{R_n}$ in the figure signify that these are the values of $C_j(v + V_{do})$ and $R_n(v + V_{do})$ averaged over one cycle of the rf voltage, v.

For a particular frequency ω and average negative resistance $\overline{R_n}$, the impedance $Z(\omega, \overline{R_n})$ will have a zero. In the numerical approximation this zero is found numerically, and in the analytical approximation a truncated series expansion of Z is solved. $\overline{R_n}$ is then related to the magnitude of v using the $I-V$ curve of the particular diode being considered.

The numerical approximation begins with a calculation of the zeros of Z using the value of C_j at the dc bias point, $C_j(V_{do})$. A value for the amplitude of v is then guessed, and an integration performed over the diode $I-V$ curve to obtain an average rf power, P, from which an estimate for $\overline{R_n}$, $\overline{R_{n,\text{est}}}$, can be found using the relation

$$\overline{R_{n,\text{est}}} = \frac{1}{2}\frac{v^2}{P} . \tag{18}$$

It is important that P be found by averaging the product of the rf voltage across the tunnel diode multiplied by the rf current through it.[53] The dc bias power must not be included.

New values of the amplitude of v are successively guessed until one is found that gives $\overline{R_{n,\text{est}}} = \overline{R_n}$. With that value and $\overline{C_j}$, a new calculation of the zero of Z must be made. These nested iterations are carried to a point of convergence within the roundoff error of the computer. The voltage across the diode is considered to have no harmonic content, whereas the harmonic content of the diode current generated by the nonlinearity of the tunnel diode is decomposed by Fourier analysis. Equations (16) and (17) are then used to calculate V_{bias} and I_{bias}.

V. ASSUMPTIONS USED IN THE NUMERICAL APPROXIMATION

In addition to the assumptions which applied to the numerical simulation, this numerical approximation method also assumes the following: (6) Nonlinear effects can be adequately accommodated by the use of the average value $\overline{R_n}$. (7) The only important harmonic effect is that the diode nonlinearity generates harmonics in the diode current. (8) The mutual inductance between the two parts of the inductor can be neglected.

VI. ANALYTIC APPROXIMATION

For the analytical approach, we write the complex equation for the impedance as a function of the components, series expand appropriately, and solve. An examination of Fig. 2 allows us to write the following equation as our starting point.

$$Z(\omega, \overline{R_n}) = \frac{1}{j\omega C} + j\omega L_2 + R_2 + \frac{1}{\dfrac{1}{R_p + \dfrac{1}{1/\overline{R_n} + j\omega(C_p + \overline{C_j})}} + \dfrac{1}{R_1 + j\omega L_1}} . \tag{19}$$

Since the algebra necessary to transform Eq. (19) into the desired answer is very involved, we will just outline the calculation here.[54] For the case of $x \ll 1$, we expand Z in the following four small quantities: $|R_1/\overline{R_n}| < 0.00001$, $|\omega L_1/\overline{R_n}| < 0.01$, $|R_p/\overline{R_n}| < 0.01$, and $|\omega C_p \overline{R_n}| < 0.1$. We then solve for $\overline{R_n}$ and ω and simplify using $Q = \omega_0 L/R$, $R = R_1 + R_2$, $L = L_1 + L_2$, $x = R_1/R = L_1/L$, and $\omega_0 = 1/(\text{LC})^{1/2}$. The result for $\overline{R_n}$ and ω is

$$\overline{R_n} = -R_p - x^2 Q\omega_0 L\left[1 + 2x\frac{C_p}{C} - 3x^2\frac{C_p}{C} - 3\omega_0^2 R_p^2 C_p^2 - x^2 Q\omega_0 R_p C_p \frac{C_p}{C} + \frac{4\omega_0 R_p C_p}{xQ} - \frac{1}{x^2 Q^2} + O(10^{-5})\right] , \tag{20}$$

$$\omega = \omega_0\left[1 - \frac{1}{2}x^2\frac{C_p}{C} - \frac{1}{2}x^3\frac{C_p^2}{C^2} - \frac{\omega_0 R_p C_p}{Q} - \frac{1}{2}\frac{\omega_0^2 R_p^2 C_p C}{x^2 Q^2} - \frac{1}{Q^2} + \frac{1}{2}\frac{1}{xQ^2} + O(10^{-8})\right] . \tag{21}$$

For the case where $x = 1$, we use the small quantities $|R/\overline{R_n}| < 0.0001$, $|\omega L/\overline{R_n}| < 0.01$, and $|R_p/\overline{R_n}| < 0.1$. Similar calculations yield

$$\overline{R_n} = -R_p - Q\omega_0 L\left[1 - Q\omega_0 R_p C_p\frac{C_p}{C} - \frac{1}{2}\frac{C_p}{C} - 3\omega_0^2 R_p^2 C_p^2 + Q^2\omega_0^2 R_p^2 C_p^2\frac{C_p^2}{C^2} + O(10^{-3})\right] , \tag{22}$$

$$\omega = \omega_0\left[1 - \frac{1}{2}\frac{C_p}{C} - \frac{\omega_0 R_p C_p}{Q} + \frac{3}{8}\frac{C_p^2}{C^2} - \frac{1}{2}\frac{\omega_0^2 R_p^2 C_p C}{Q^2} - \frac{1}{2}\omega_0^2 R_p^2 C_p^2\frac{C_p}{C} - \frac{1}{2}\frac{1}{Q^2} + O(10^{-5})\right] . \tag{23}$$

Downloaded 25 May 2011 to 128.227.27.199. Redistribution subject to AIP license or copyright; see http://rsi.aip.org/about/rights_and_permissions

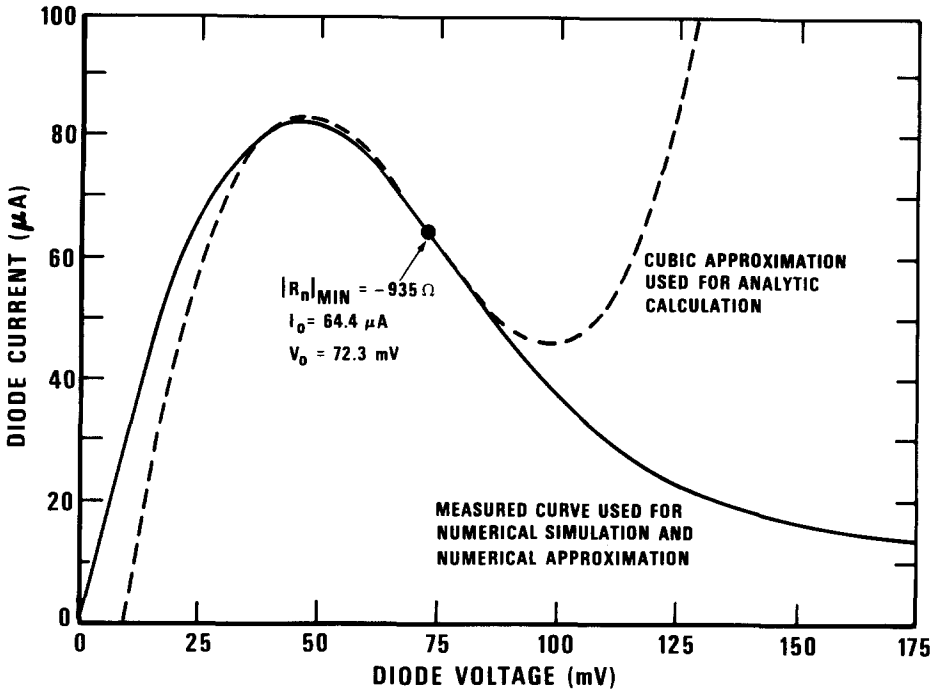

FIG. 3. The current–voltage characteristic of the tunnel diode and its cubic approximation.

Comparison of Eq. (20) with Eq. (22) and of Eq. (21) with Eq. (23) shows that, without loss of accuracy, we may combine these pairs of formulas into the following single pair:

$$\overline{R_n} = -R_p - x^2 Q\omega_0 L\Big(1 + 2x\frac{C_p}{C} - 3x^2\frac{C_p}{C} + \frac{1}{2}x^3\frac{C_p}{C} - 3\omega_0^2 R_p^2 C_p^2 - x^2 Q\omega_0 R_p C_p\frac{C_p}{C} + x^4 Q^2\omega_0^2 R_p^2 \times C_p^2\frac{C_p^2}{C^2} + \frac{4\omega_0 R_p C_p}{xQ} - \frac{1}{x^2Q^2} + \cdots\Big), \quad (24)$$

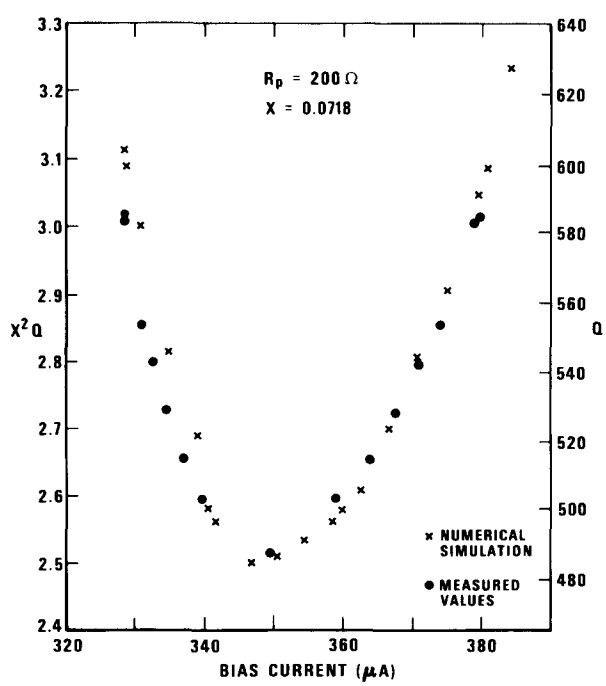

FIG. 4. Comparison of the experimental and simulation results for values of x^2Q at the threshold of oscillation.

$$\omega = \omega_0\Big(1 - \frac{1}{2}x^2\frac{C_p}{C} - \frac{1}{2}x^3\frac{C_p^2}{C^2} + x^4\frac{C_p^2}{C^2} - \frac{1}{8}x^5\frac{C_p^2}{C^2} - \frac{\omega_0 R_p C_p}{Q} - \frac{1}{2}\frac{\omega_0^2 R_p^2 C_p C}{x^2Q^2} - \frac{1}{2}x^2\omega_0^2 R_p^2 C_p^2\frac{C_p}{C} - \frac{1}{Q^2} + \frac{1}{2}\frac{1}{xQ^2} + \cdots\Big). \quad (25)$$

For $x = 1, Q > 100, C_p/C < 0.01$, and $|R_p/R_n| < 0.1$, additional terms in the series of Eq. (24) are of the order of 1000 ppm, and additional terms in the series of Eq. (25) are of the order of 10 ppm. Similarly, for $0.15 > x > 0.05$, $Q > 1000$, $C_p/C < 0.01$, and $|R_p/\overline{R_n}| < 0.1$, the corresponding values are 10 ppm and 0.01 ppm. We have not calculated any formulas which are valid for $x \ll 0.05$.

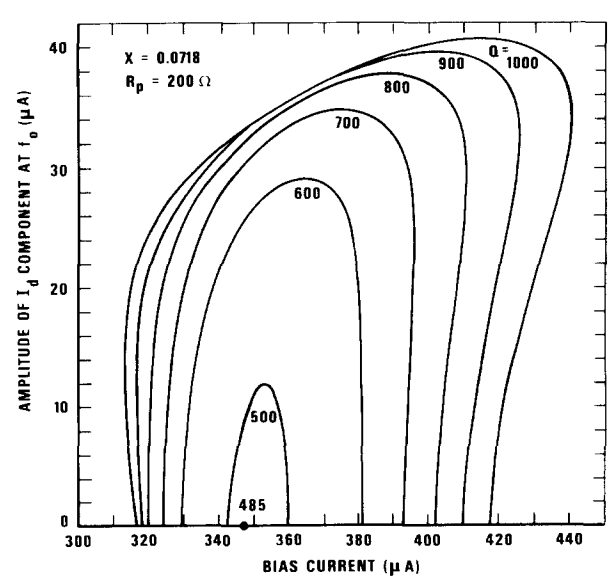

FIG. 5. Amplitude of the fundamental component of the current through the tunnel diode vs dc bias current as Q is increased beyond its threshold value.

Downloaded 25 May 2011 to 128.227.27.199. Redistribution subject to AIP license or copyright; see http://rsi.aip.org/about/rights_and_permissions

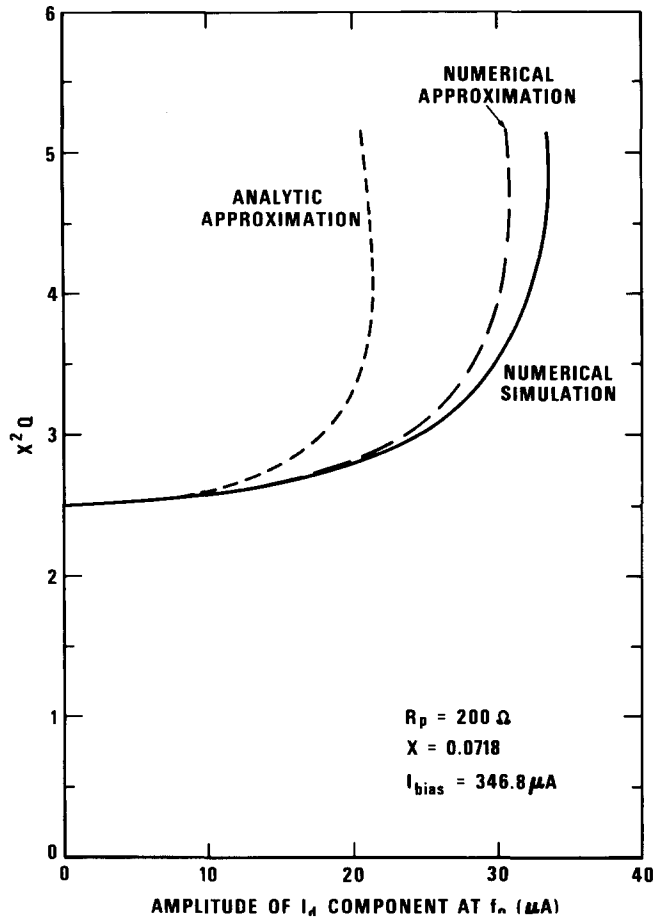

FIG. 6. Comparison of the results of the three methods of calculating the amplitude of the fundamental component of the current through the tunnel diode as x^2Q is changed.

Equation (25) is seen to have a term which varies as $1/Q$ as well as terms with the expected $1/Q^2$ dependence. If $x = 1$, then R_p could be zero, and the $1/Q$ dependence would drop out. The Q dependence would then be as

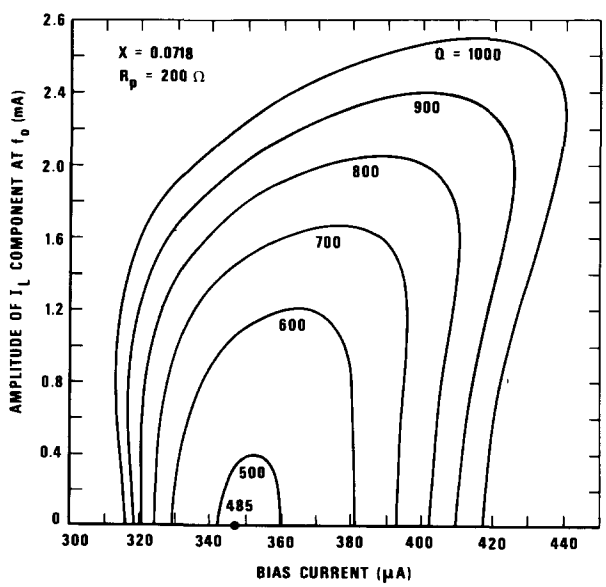

FIG. 7. Amplitude of the fundamental component of the current through the inductor of the LC circuit as a function of the dc bias current.

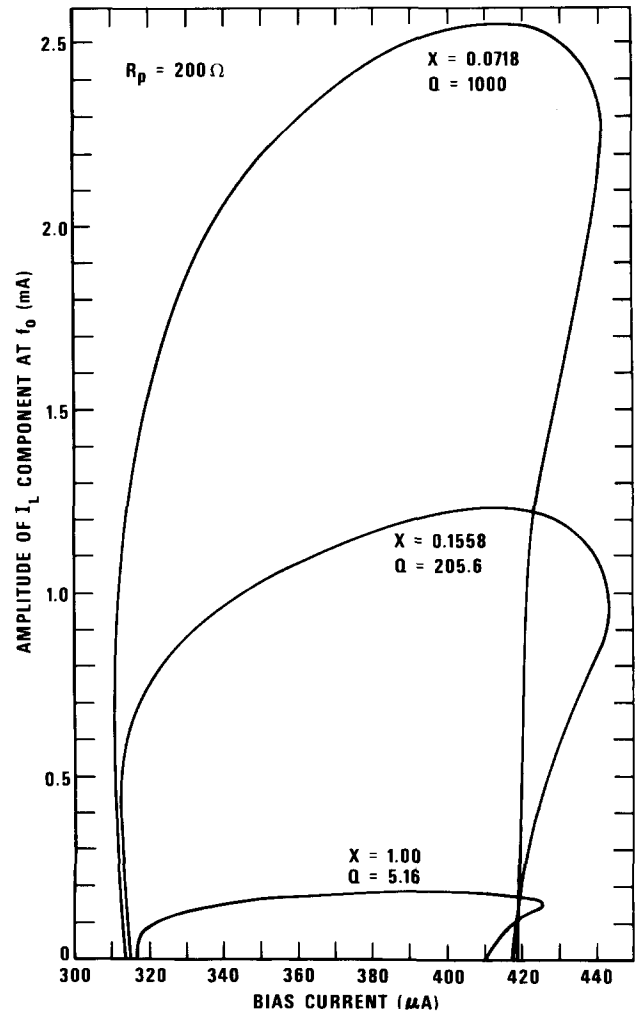

FIG. 8. The variation of the fundamental component of the current in the inductor as the tapping fraction and Q are changed in a manner which keeps the rf power and nonlinear effects nearly constant (x^2Q = constant).

predicted by simple calculations. As a practical matter, however, low-temperature multiturn inductor circuits have Q values so high that if $x = 1$, the circuit would be greatly overdriven by any available tunnel diode, and nonlinear effects would be more important than the $1/Q^2$ term. If, on the other hand, the diode impedance is matched to the resonator by letting x be less than 1, it will be necessary to have R_p nonzero in order to suppress parasitic oscillations and the $1/Q$ term will dominate. We therefore contend that for low-temperature circuits with multiturn inductors, there is never an actual circuit where the $1/Q^2$ term alone is applicable. For room temperature multiturn inductor circuits or for reentrant resonator circuits, however, the value of $Q\omega L$ is so small that available tunnel diodes can be properly matched with $x = 1$ and the $1/Q^2$ term can dominate.

In order to relate $\overline{R_n}$ to the amplitude of the rf current through the tunnel diode, we use a cubic approximation of the tunnel diode I–V curve.

$$I_d(V_d) = I_{do} + \frac{V_d - V_{do}}{R_{no}} - \frac{(V_d - V_{do})^3}{3R_{no}(V_{\text{peak}} - V_{do})^2}, \quad (26)$$

Downloaded 25 May 2011 to 128.227.27.199. Redistribution subject to AIP license or copyright; see http://rsi.aip.org/about/rights_and_permissions

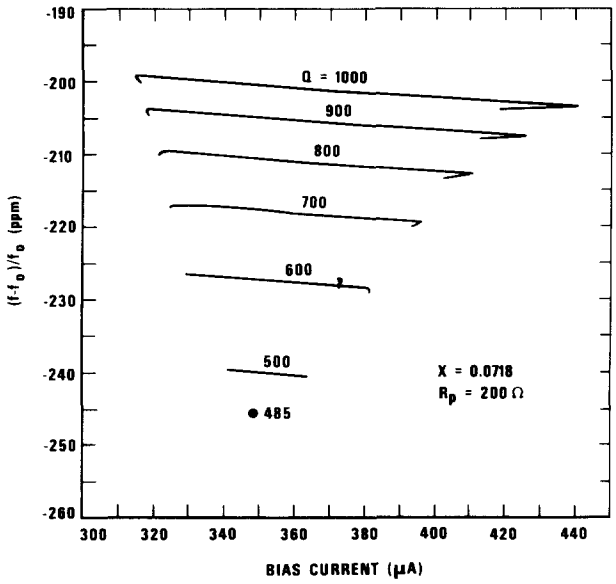

FIG. 9. Relative frequency shift from $f_0 = \frac{1}{2}\pi(LC)^{1/2}$ as a function of the dc bias current for a tapping fraction of 0.0718.

where V_{peak} is the voltage of the current peak in the I-V curve.

This equation and the true $I-V$ curve for the particular diode we consider in this paper are shown in Fig. 3.

When the diode is biased at its inflection point, the amplitude of the rf current through it is then given by

$$i_d = 2\left|\frac{V_{do} - V_{\text{peak}}}{\overline{R_n}}\right|(1 - R_{no}/\overline{R_n})^{1/2}. \tag{27}$$

In deriving this relation care has been taken to interpret $\overline{R_n}$ using Eq. (18) with $\overline{R_n} = \overline{R_{n,\text{est}}}$.

The current through the inductor can be calculated by equating the power supplied by the diode with the power dissipated by the resistance of the resonator. The result is

$$i_L = xQi_d. \tag{28}$$

VII. ASSUMPTIONS USED IN THE ANALYTIC APPROXIMATION

In addition to the assumptions made for the numerical simulation and numerical approximation methods, we have assumed that certain quantities are small and used a

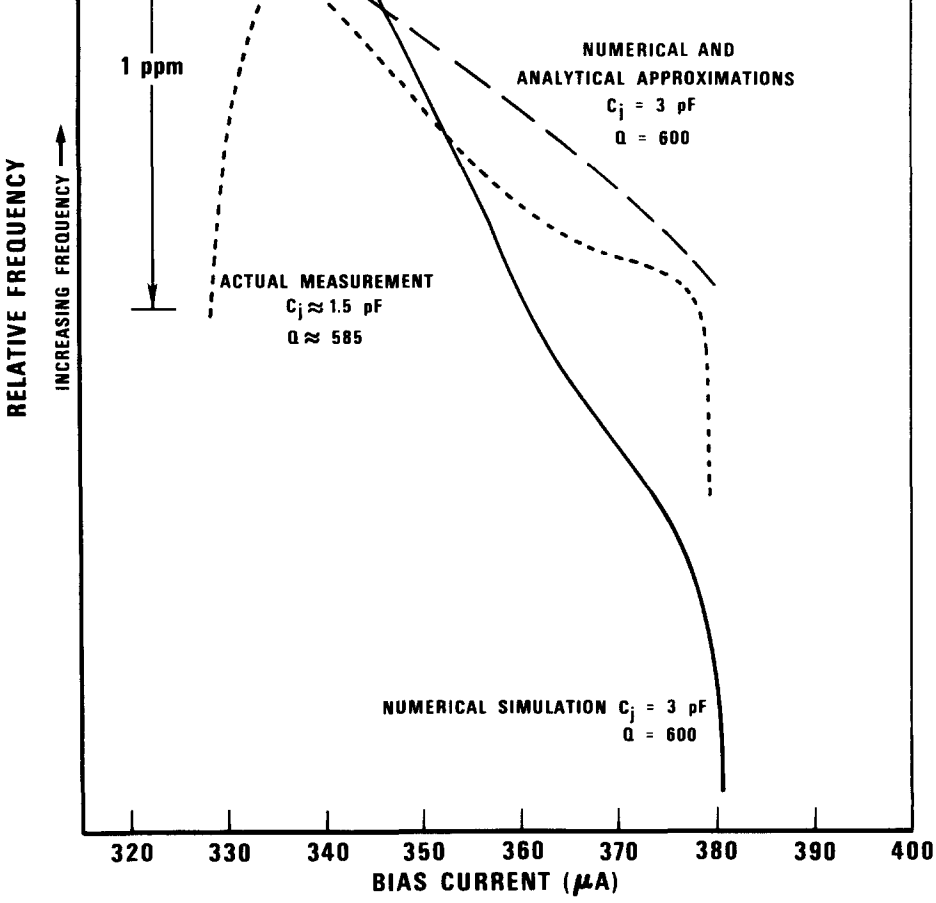

FIG. 10. Comparison of measured frequency vs dc bias current with results calculated using the three methods. These curves are plotted in close proximity to allow comparison of their shapes. In actuality they are displaced from each other by several parts per million as is shown in Table I. Differences between the shapes of numerical and analytical approximation method results are, however, still too small to show in this figure.

Downloaded 25 May 2011 to 128.227.27.199. Redistribution subject to AIP license or copyright; see http://rsi.aip.org/about/rights_and_permissions

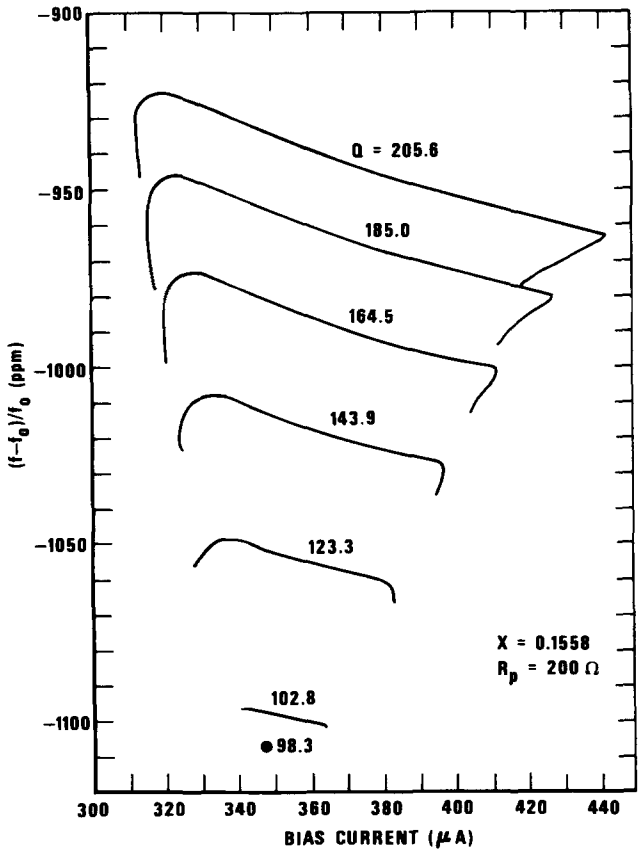

FIG. 11. Relative frequency shift from f_0 vs dc bias current at a tapping fraction of 0.1558.

cubic approximation to the $I-V$ curve. These are detailed below Eq. (25) and need not be repeated here. In applications where they have values outside these limits, the results will certainly be less accurate although still useful.

VIII. RESULTS

We studied five different combinations of tapping fraction and parasitic suppression resistance: $x = 0.0718$, $R_p = 200\ \Omega$; $x = 0.1558$, $R_p = 200\ \Omega$; $x = 0.25$; $R_p = 400\ \Omega$; $x = 1$, $R_p = 200\ \Omega$; and $x = 1$, $R_p = 0$. For all but the $x = 0.25$ case, we examined the entire region of oscillation using values of Q up to over twice the value of Q at the threshold. For the $x = 0.25$ case, we only identified the threshold and observed that a parasitic oscillation occurred for $x = 0.25$ and $R_p = 200\ \Omega$. The $x = 0.0718$ case was given particular attention since it has nearly the correct parameters for simulation of an actual oscillator for which we have extensive experimental measurements.[30] The remaining cases were calculated to aid in our understanding of tunnel diode oscillators and to compare with corresponding numerical approximation and analytic approximation calculations. For this purpose, the $x = 1$ cases are very useful, even though actual oscillators with such low Q would be of questionable value.

Our results are illustrated graphically in Figs. 4–13 and numerically in Table I. The figures show different aspects of the numerical simulation with Figs. 4 and 10 also showing experimental data, and Figs. 6 and 10 also showing comparisons between the numerical simulation and the numerical and analytical approximations. The table serves to illustrate the errors which result, if the numerical and analytical approximations are used in place of the full numerical simulation.

In Fig. 4 we compare the oscillation threshold points calculated by the numerical simulation (crosses) with actual measurements (solid circles). Although the circuit bias current, I_{bias}, which forms the abscissa can be accurately measured, the unloaded circuit Q is difficult to measure with better than 10% accuracy. When we did make passive measurements of the circuit Q in a separate run, we obtained values lower than those plotted for the data by 5%. Therefore, to accommodate this likely systematic error and to allow better comparison of the shapes of the calculated and experimental curves, we uniformly shifted all experimental Q values up by 5%. It can be seen that the agreement in the shapes is quite good, although below 340 μA, there appears to be a systematic error. We believe that this is caused by slight differences between the true $I-V$ curve and the $I-V$ curve used by the simulation program which interpolated[55] between measured points spaced every 5 mV. With our

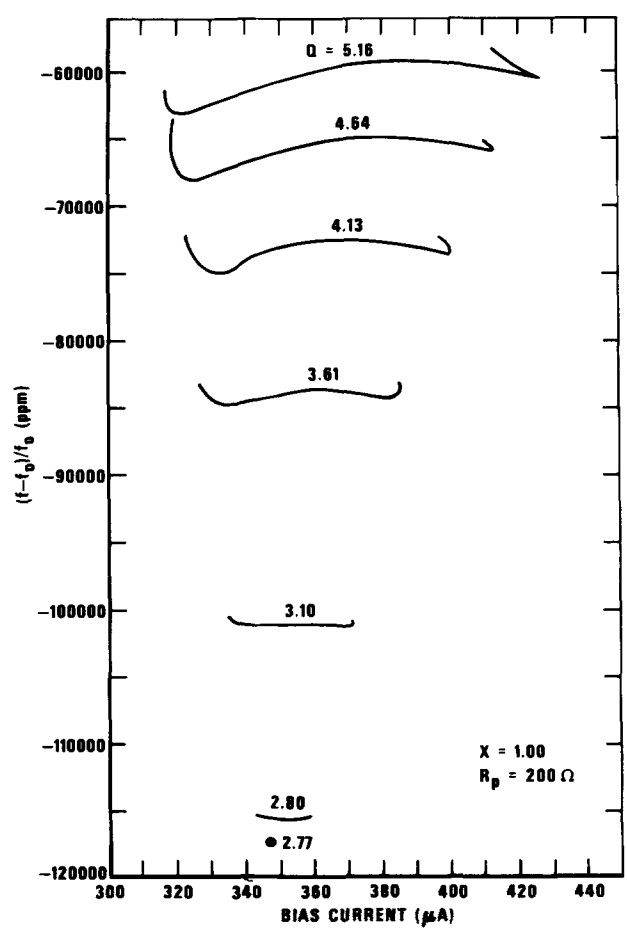

FIG. 12. Relative frequency shift from f_0 vs dc bias current at a tapping fraction of 1.000. Note how the ends of these curves turn in the opposite direction to that shown in Figs. 9 and 11 for lower values of tapping fraction.

Downloaded 25 May 2011 to 128.227.27.199. Redistribution subject to AIP license or copyright; see http://rsi.aip.org/about/rights_and_permissions

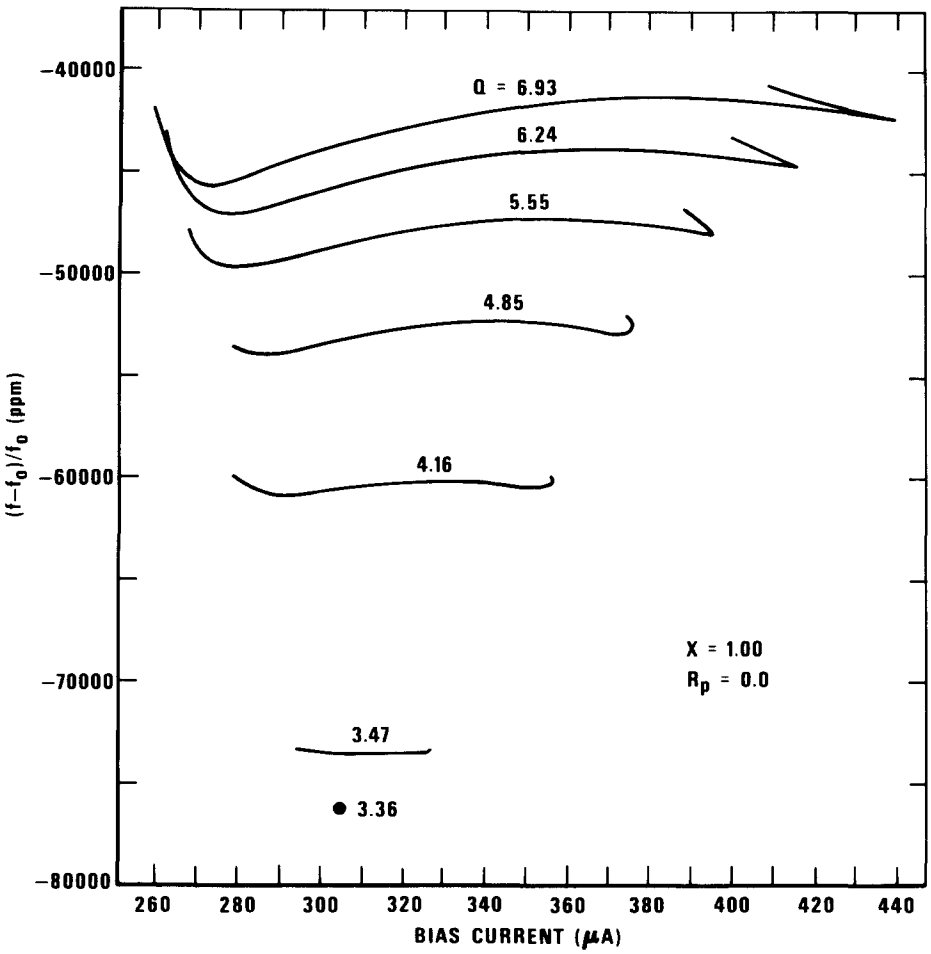

Fig. 13. This is the same as Fig. 12, except that the parasitic suppression resistance has been reduced from 200 Ω to 0. By comparing this figure with Fig. 12, one can see how a nonzero value for R_p narrows the range of oscillation while allowing a lower threshold Q value.

confidence in the numerical simulation boosted by this and other tests, we believe that measurement of the bias characteristics and simulation of the oscillator may be a better way to determine the circuit Q than a direct experimental measurement. The oscillator transforms the Q, with very little loading, to an effect in the frequency-bias characteristic. By measuring the oscillator drop out and restart bias points, we can observe changes in x^2Q as small as 0.1%. A direct measurement, on the other hand, must have rf cables coupled to the circuit, impedance measurements made by external instrumentation, and calculated corrections.

Whereas Fig. 4 shows the Q dependence of the threshold of oscillation, Fig. 5 shows the behavior of the amplitude of the fundamental component of the current through the tunnel diode, I_d, as a function of I_{bias} for selected Q values. Figure 4 can be seen to be a slice through Fig. 5 at $I_d = 0$ μA. The most striking feature of Fig. 5 is its multivalued nature. There exist regions (e.g., at 420 μA and $Q = 1000$) where two amplitudes are shown for a single value of dc bias current. When this is the case, the lower amplitude is unstable and the oscillation will grow until the larger amplitude is attained. If, however, the oscillator were biased at 420 μA, but not oscillating at all, it would not spontaneously start oscillating until the bias was lowered below 418 μA. This is the hysteretic behavior mentioned earlier which is caused by the self-rectification of the rf current by the nonlinearities of the tunnel diode. The other noteworthy features of Fig. 5 are the saturation at values for $I_d > 32$ μA and the asymmetry about the threshold point of 346.8 μA. Both of these effects are the direct result of the shape of the tunnel diode $I-V$ characteristic as may be seen by examination of Fig. 3 and noting that 32 μA corresponds to an rf voltage of about 30 mV.

Figure 6 shows a vertical slice of Fig. 5 at 346.8 μA (solid curve) together with equivalent results from the analytic (short dashes) and numerical approximations (long dashes). The primary error of the analytic approximation is its use of a cubic approximation for the tunnel diode $I-V$ curve. It is apparent when one compares the two curves in Fig. 3 that the cubic approximation forces the analytic approximation to underestimate I_d. The numeric approximation is much better, but its coarse treatment of harmonic effects and neglect of mutual inductance cause it also to underestimate I_d.

The current through the inductor, i_L, is shown in Figs. 7 and 8. Figure 7 illustrates how i_L varies with dc bias and Q, whereas Fig. 8 shows how it varies with x for approximately constant values of x^2Q. We have used Eq. (28) to compare i_L with I_d and find that it overestimates i_L by only 7% when it is applied to all numerical simulation results, irrespective of x and R_p.

The results describing the frequency vs circuit bias are shown in Figs. 9–13. Figure 9 shows the typical behavior for small values of x. The threshold point has

Downloaded 25 May 2011 to 128.227.27.199. Redistribution subject to AIP license or copyright; see http://rsi.aip.org/about/rights_and_permissions

TABLE I. Comparison of the results obtained by the analytical approximation (A.A.), numerical approximation (N.A.), and numerical simulation (N.S.) methods. The $x = 0.0718$ circuit closely approximates the actual oscillator used in Ref. 30.

			$(f - f_0)/f_0$ (ppm)			i_d (μA)		
x	R_p (Ω)	Q	A.A.	N.A.	N.S.	A.A.	N.A.	N.S.
0.0718	200	485	−230.3	−230.7	−242.0	3.4	3.3	1.0
		500	−228.8	−230.1	−239.8	8.9	10.3	9.1
		600	−218.9	−220.1	−227.2	18.5	24.8	26.0
		700	−211.3	−212.5	−217.5	20.8	28.9	30.6
		800	−205.5	−206.6	−210.6	21.3	30.4	32.5
		900	−200.8	−202.0	−209.8	21.0	30.8	33.5
		1000	−197.0	−198.2	−200.5	20.3	30.6	33.4
0.1558	200	98.3	−1002.7	−1006.2	−1107.	0.0	0.0	1.0
		102.8	−998.7	−1006.6	−1097.	5.4	5.1	12.5
		123.3	−978.7	−985.7	−1052.	17.9	23.8	26.0
		143.9	−958.9	−965.5	−1013.	20.7	28.5	30.5
		164.5	−941.4	−947.5	−981.	21.3	30.3	32.4
		185.0	−926.0	−932.0	−956.	21.1	30.8	33.2
		205.6	−912.6	−918.5	−933.	20.5	30.7	33.4
0.2500	400	29.26	−4660.	−4743.	−5050.	6.6	4.8	1.0
1.0000	200	2.77	−111239.	−117143.	−117500.	0.0	3.0	1.0
		2.80	−109651.	−115353.	−115520.	0.0	5.6	6.2
		3.10	−96141.	−100277.	−101250.	15.2	19.7	19.6
		3.61	−80204.	−82829.	−84250.	20.0	26.8	27.3
		4.13	−69450.	−71253.	−73480.	21.2	29.6	30.6
		4.64	−62085.	−63416.	−66200.	21.2	30.6	32.4
		5.16	−56614.	−57642.	−61000.	20.7	30.8	33.1
1.0000	0	3.36	−73503.	−76033.	−76200.	0.0	0.0	1.0
		3.47	−70740.	−73161.	−73400.	0.0	11.5	11.0
		4.16	−58107.	−59634.	−60500.	18.7	25.7	26.3
		4.85	−50471.	−51553.	−53200.	21.1	28.8	29.9
		5.55	−45447.	−46276.	−48600.	21.0	29.4	31.0
		6.24	−42056.	−42730.	−45600.	20.2	29.0	31.2
		6.93	−39626.	−40198.	−43600.	19.1	28.2	30.7

the greatest frequency shift from $f_0 = \frac{1}{2}\pi(LC)^{1/2}$. As the Q is increased the frequency approaches f_0. The hysteretic behavior is evident as producing hooks at the ends of the curves.

Figure 10 shows a comparison between equivalent results for $x = 0.0718$, $R_p = 200\ \Omega$, $C_j = 3$ pF, and $Q = 600$ for the three methods of calculations. Only the numerical simulation (solid line) has the qualitative behavior evident in the curve representing actual measurements (short dashes) on a similar oscillator ($x = 0.0718$, $R_p = 200\ \Omega$, $C_j = 1.5$ pF, and $Q = 585$). The analytic and numerical approximations have the same shape (long dashes). These curves are plotted in close proximity to allow comparison of their shapes. In actuality they are displaced from each other by several parts per million as is shown in Table I.

Figures 9, 11, and 12 illustrate how much the shape and spread of these curves of frequency shift vs dc bias current change as the tapping fraction is changed. Even the direction that the end points turn reverses as the tapping fraction is raised from 0.1558 to 1.0. The values chosen for Q in these figures have been selected to maintain x^2Q approximately constant, thereby better illustrating the effect of the nonlinearities.

When $x = 1$, there is usually no need for any parasitic suppression resistor. We have therefore shown the effect of removing R_p from the circuit in Figs. 12 and 13. The width of circuit bias current over which oscillation occurs is broadened and the threshold Q is raised. At first glance, it is quite surprising that inserting a resistance into the circuit can allow the tunnel diode to make lower Q circuits oscillate. One does not get something for nothing. The nonlinear effects become more severe at smaller amplitudes, and the frequency becomes more sensitive to the dc bias current. We do not recommend inserting a value for R_p solely to make a given tunnel diode drive a lower Q circuit. Instead, one should get a more powerful tunnel diode and use the smallest value for R_p which is necessary to suppress parasitic oscillations.

Table I quantitatively shows how the analytic approximation (A.A.), numerical approximation (N.A.), and numerical simulation (N.S.) methods compare in predicting the frequency shift and diode rf current when the diode is biased at its inflection point. It serves to let the user of the approximation methods estimate the direction and magnitude of the errors in the approximation. As can be seen in the table, for $x < 0.1$ or $x = 1$ and high values of Q, the numerical simulation and numerical approximation methods agree very well, particularly in the prediction of the frequency shift.

Unintended oscillations at frequencies other than f_0 are called parasitic oscillations, since they are made possible by stray capacitances and inductances and take power away or even inhibit the desired oscillation. At $x = 0.25$ and $R_p = 200\ \Omega$, we observed that TDO would

Downloaded 25 May 2011 to 128.227.27.199. Redistribution subject to AIP license or copyright; see http://rsi.aip.org/about/rights_and_permissions

not converge to a steady-state solution. The reason was simply that R_p was too small to suppress a parasitic oscillation caused by resonance of L_1 and C_p at a frequency 16 times greater than f_0. The integration mesh was too coarse to resolve the higher frequency of the parasitic oscillation. As soon as we used $R_p = 400\ \Omega$, TDO converged with no difficulty. The numerical and analytical approximation methods will reveal parasitic oscillations only when reformulated to examine specific parasitic resonances.

IX. OTHER APPROACHES AND EXTENSIONS

Although the methods and results presented in this paper are useful and practical, they can still be greatly expanded. We have not dealt with noise effects and have neglected some circuit parameters which will become important at higher frequencies. Furthermore, the analytic approach can be carried to higher orders by systematic methods described in the literature of nonlinear periodic differential equations.[40,41,56–60]

It is clear that at very small amplitudes of oscillation, the frequency noise will be larger because of a poor ratio of signal power to noise power. Furthermore, at very large amplitudes the flat portions of the diode $I-V$ curve at the peak and valley will contribute additional shot noise. Also the nonlinearities will mix in off-resonance noise power. There must be an optimum amplitude for oscillation between 5 and 20 mV rms. It would be desirable to be able to calculate this optimum quantitatively and confirm it experimentally.

We believe that we have carried the frequency shift and amplitude calculations to the point where their usefulness is limited by the accuracy with which the circuit parameters can be experimentally measured. At the frequencies where reentrant resonators can be conveniently used as LC resonators, precise characterization of the equivalent circuits of the diode, bypass capacitor, and resonator coupling loop are difficult even with the availability of a microwave network analyzer.

An important topic which we have not thoroughly investigated is the effect that parasitic resonances can have when their oscillation is just barely suppressed. How far under the threshold for oscillation must a parasitic resonance be for it to have no important effect? Presently, we just assume that if parasitic resonances have Q values less than one half their threshold values, they will not significantly disturb the circuit.

ACKNOWLEDGMENTS

It is a pleasure to thank Dr. Marilyn Bishop for bringing to our attention the differential equation solution routine. The particularly useful comments of NBS reviewers Robert D. Cutkosky and Dr. Gary P. Carver were appreciated. We also wish to acknowledge NSF Grant #DMR 74-20310 for supporting the experimental measurements and numerical simulation calculations when the authors were at the University of California, Irvine.

[1] L. Mills and S. G. Sydoriak, Ann. Phys. (NY) **34**, 276 (1965).
[2] John F. Jarvis, Dietolf Ramm, and Horst Meyer, Phys. Rev. **170**, 320 (1968).
[3] E. J. Yarmchuk and W. I. Glaberson, J. Low Temp. Phys. **36**, 381 (1979).
[4] C. T. Van Degrift, W. J. Bowers, Jr., D. G. Wildes, and P. B. Pipes, Instrum. Soc. Am. Trans. **19**, 15 (1980).
[5] M. Sudraud and Eric Varoquaux, C. R. Acad. Sc. Paris **278**, 921 (1974).
[6] Gregory Goeliner and Horst Meyer, Phys. Rev. Lett. **26**, 1534 (1971).
[7] C. Boghosian, H. Meyer, and J. E. Rives, Phys. Rev. **146**, 110 (1966).
[8] B. A. Wallace, Jr. and H. Meyer, J. Low Temp. Phys. **15**, 297 (1974).
[9] Craig T. Van Degrift, "Dielectric Constant, Density, and Expansion Coefficient of Liquid He-4 at Vapor Pressure Below 4.4 K," Ph.D. thesis No. 74-19243 (1974), University Microfilms, 300 North Zeeb Road, Ann Arbor, Michigan 48106.
[10] A. Kakizaki, J. Low Temp. Phys. **24**, 67 (1976).
[11] E. H. Graf, D. M. Lee, and John D. Reppy, Phys. Rev. Lett. **19**, 417 (1967).
[12] H. Dandache and A. Briggs, J. Low Temp. Phys. **29**, 275 (1977).
[13] Martin E. Banton, J. Low Temp. Phys. **16**, 211 (1974).
[14] H. A. Notarys, Phys. Rev. Lett. **20**, 258 (1968).
[15] B. M. Oliver and R. M. Clements, J. Phys. E (GB) **5**, 718 (1972).
[16] R. H. Willens, E. Buehler, and E. A. Nesbitt, Rev. Sci. Instrum. **39**, 194 (1968).
[17] R. B. Clover and W. P. Wolf, Rev. Sci. Instrum. **41**, 617 (1970).
[18] R. T. Harley, J. C. Gustafson, and C. T. Walker, Cryogenics **10**, 510 (1970).
[19] K. Andres and E. Bucher, J. Low Temp. Phys. **9**, 267 (1972).
[20] F. Rothwarf and D. Ford, Rev. Sci. Instrum. **43**, 317 (1972).
[21] F. Habbal, G. E. Watson, and P. R. Elliston, Rev. Sci. Instrum. **46**, 192 (1975).
[22] D. S. Greywall, Phys. Rev. B **15**, 2604 (1977).
[23] J. Aslam and W. Weyhmann, Rev. Sci. Instrum. **44**, 71 (1973).
[24] F. N. H. Robinson, J. Phys. E. (GB) **10**, 254 (1977).
[25] Craig T. Van Degrift and Donald B. Utton, U.S. Patent No. 4,087,738 (1978).
[26] A. T. Skjeltorp and W. P. Wolf, Phys. Rev. B **8**, 215 (1973).
[27] J. W. Baker, J. D. Lejeune, and D. G. Naugle, J. Appl. Phys. **45**, 5043 (1974).
[28] J. D. Lejeune and D. G. Naugle, J. Low Temp. Phys. **22**, 425 (1976).
[29] C. Varmazis and Myron Strongin, Phys. Rev. B **10**, 1885 (1974).
[30] David P. Love, "Temperature Dependence of the Electronic Relaxation Time in Copper, Aluminum, and Potassium Determined from Changes in the Surface Impedance at Low Temperatures," Ph.D. thesis No. 79-06402 (1978), University Microfilms, 300 North Zeeb Road, Ann Arbor, Michigan 48106.
[31] A. K. Drukier and L. C. L. Yuan, Nucl. Instrum. Methods **138**, 213 (1976).
[32] A. K. Drukier, J. Igalson, and L. Sniadower, Nucl. Instrum. Methods **154**, 91 (1978).
[33] H. R. Lowry, J. Giorgis, E. Gottlieb, and R. C. Weischedel, "Tunnel Diode Manual" (Semiconductor Products Department, General Electric Company, New York, 1961), pp. 33–42.
[34] Woo F. Chow, "Principles of Tunnel Diode Circuits" (Wiley, New York, 1964), pp. 151–182.
[35] Anthony S. Manera, *Solid State Electronic Circuits: for Engineering and Technology* (McGraw–Hill, New York, 1973), pp. 614–623.
[36] Kern K.N. Chang, *Parametric and Tunnel Diodes* (Prentice–Hall, Englewood Cliffs, New Jersey, 1964), pp. 157–163.
[37] D. K. Roy and B. R. Pamplin, *Tunnelling and Negative Resistance Phenomena in Semiconductors* (Pergamon, New York, 1977), pp. 94–95.
[38] Walter A. Sowa and James M. Toole, *Special Semiconductor Devices* (Holt, Rinehart and Winston, New York, 1968), pp. 92–95.
[39] V. S. Andreyev, Radiotekhnika (Moscow). Trans. Radio Eng. **25**, 107 (1970).
[40] J. Chiba, K. Honma, and T. Takano, Denki Gakkai Ronbunshi **92C**, 384 (1972). Trans. Electr. Eng. (Jpn) **92**, 122 (1972).
[41] S. Mahapatra and J. S. Joshi, Int. J. Electron. **35**, 169 (1973).
[42] V. A. Kozlov, D. Ya. Tamarchak, and Yu. L. Khotuntsev, Radiotekh. Elektron. **19**, 2002 (1974); Trans. Radio Eng. Electron. Phys. **19**, 133 (1974).
[43] F. Kourzhil and V. Rzhichnyi, Izv. Vuz Radioelektron. **19**, 58 (1976).
[44] Craig T. Van Degrift, Rev. Sci. Instrum. **46**, 599 (1975).
[45] Craig T. Van Degrift, Rev. Sci. Instrum. **45**, 1171 (1974).
[46] We performed these calculations using the PASCAL language and operating system (Univ. Calif., San Diego) on a North Star Horizon (Berkeley, California) microcomputer. Copies of our program are available.
[47] See Addendum 2 of Ref. 30 above.
[48] Fred T. Krogh, Report #NPO-11643 entitled "VODQ/SVDQ/DVDQ,

Downloaded 25 May 2011 to 128.227.27.199. Redistribution subject to AIP license or copyright; see http://rsi.aip.org/about/rights_and_permissions

Variable Order Integrators for the Numerical Solution of Ordinary Differential Equations," Jet Propulsion Laboratory, May 1, 1969.

[49] Frederick W. Grover, Proc. IRE **21**, 1039 (1933).

[50] Even when $x = 1$, a nonzero value for R_p may be required to suppress parasitic oscillation of helical resonances in a multiturn inductor.

[51] Forman S. Acton, *Numerical Methods that Work* (Harper & Row, New York, 1970), pp. 228–233.

[52] Maurice Yunik, *Design of Modern Transistor Circuits* (Prentice–Hall, Englewood Cliffs, New Jersey, 1973), pp. 309–339.

[53] One might naively believe that $\overline{R_n}$ should be the average of R_n over one cycle of the rf, rather than defined through the power by Eq. (18). Further thought, however, shows that power is a more fundamental quantity than resistance and that resistance is only a convenient shorthand notation for power loss (when positive) or power generation (when negative). This is similar to the definitions of capacitance and inductance being based on energy storage by electric charges and currents rather than the conventional geometric formulations. If one tries to use the average of R_n, the divergences of R_n at the peak and valley points of the tunnel diode $I-V$ curve will be weighed too strongly.

[54] Details of the analytic calculations may be obtained from the authors.

[55] After all of the calculations by TDO were completed, we found an error in the interpolation routine which calculated $I_d(V_d)$ from the measured $I-V$ curve data for the diode used in the experiment. Instead of performing the four point interpolation with two data points on each side of V_d, the routine used one point on one side and three points from the other side. The error thus incurred was quite small and nearly lost in the uncertainty of the data points. Nevertheless, when making comparisons between the numerical simulation and numerical approximation methods, it was quite important to use the same function $I_d(V_d)$. We therefore intentionally used an identical erroneous interpolation when calculating $I_d(V_d)$ for the numerical approximation. A recalculation of the numerical simulation with this interpolation error corrected would be expensive and not change any results significantly.

[56] Ali Hasan Nayfeh and Dean T. Mook, *Non-linear Oscillations* (Wiley, New York, 1979).

[57] Minoru Urabe, *Non-linear Autonomous Oscillations—Analytical Theory* (Academic, New York, 1967).

[58] Dragoslav D. Siljak, *Non-linear Systems—The Parameter Analysis and Design* (Wiley, New York, 1969).

[59] Austin Blaquiere, *Non-linear System Analysis* (Academic, New York, 1966).

[60] Nicholas Minorsky, *Non-linear Oscillations* (Van Nostrand, Princeton, New Jersey, 1962).

Downloaded 25 May 2011 to 128.227.27.199. Redistribution subject to AIP license or copyright; see http://rsi.aip.org/about/rights_and_permissions